TROPICAL CYCLONE PRECIPITATION TYPES OBSERVED BY MICROWAVE SPACEBORNE AND AIRBORNE INSTRUMENTATION

Robbie E. Hood[*]
NASA / Marshall Space Flight Center, Huntsville, Alabama

Daniel Cecil
University of Alabama in Huntsville, Huntsville, Alabama

Frank J. LaFontaine
Raytheon ITSS, Huntsville, Alabama

1. Introduction

Space-based observations of precipitation offer great promise for improved understanding and quantitative estimation of tropical cyclone rainfall. The fulfillment of this promise will play a significant role in addressing key National Aeronautics and Space Administration (NASA) Earth Science research goals of monitoring global precipitation changes, explaining correlations of these possible changes to global climate change, and improving weather forecasting, which are a subset of a larger set of goals outlined by Asrar et al. (2001). This promise will also contribute to the U.S. Weather Research Program goal of accurate 72-h prediction of landfalling hurricane rainfall discussed by Elsberry (2002).

To identify the potential of spaceborne microwave observations to map tropical cyclone (TC) rainfall, a study of TC precipitation type has been undertaken using microwave observations from both spaceborne and airborne instrumentation. Tropical cyclones sampled by the Tropical Rainfall Measuring Mission (TRMM) and the ER-2 high altitude aircraft as part of the Third Convection And Moisture EXperiment (CAMEX-3) in 1998 and the Fourth Convection And Moisture Experiment (CAMEX-4) in 2001 form the basis of this study. Highlights of complimentary TRMM and CAMEX-3 observations of Hurricane Bonnie are presented here.

2. Spaceborne and airborne observations

After becoming a hurricane on 22 August 1998 north of eastern Hispaniola, Hurricane Bonnie, as reported by Lixion Avila of the National Hurricane Center (http://www.nhc.noaa.gov/1998bonnie.html), made landfall at Wilmington, North Carolina on 26 August as a hybrid category 2/3 storm. The TRMM satellite passed over Hurricane Bonnie at approximately 1134, 1311, and 1448 UTC before and during the North Carolina landfall. Simultaneously, the NASA ER-2 high altitude aircraft carrying passive and active microwave instrumentation performed

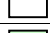multiple overpasses of Hurricane Bonnie between 1120 – 1720 UTC.
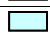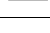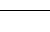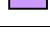
Surface rainfall rates and precipitation types for Hurricane Bonnie have been extracted from the standard orbital TRMM satellite products compiled using TRMM Microwave Imager (TMI) and Precipitation Radar (PR) information. (See Kummerow et al. (2000) for a summary of TMI and PR instrument characteristics and a complete listing of the TRMM standard products.) By contrast, an aircraft rainfall algorithm has been developed for this study using Advanced Microwave Precipitation Radiometer (AMPR) observations collected by the ER-2 aircraft. The AMPR is a total power passive microwave radiometer producing calibrated brightness temperatures (TB) at 10.7, 19.35, 37.1, and 85.5 GHz. A more complete description of the instrument may be found in Spencer et al., (1994).

The AMPR rainfall algorithm utilizes these four brightness temperatures to produce a single precipitation index at each AMPR footprint. This index reflects the magnitude of liquid rain and the magnitude of precipitation ice aloft. The indices are listed in Table 1 and are mapped in Fig. 1 for the oceanic portions of the 26 August 1998 Hurricane Bonnie flight. As listed in Table 1, precipitation index values of 1-4 indicate a possibility of clouds or very light rain due to microwave emission by small drops warming the 85 GHz TB. These are mapped in shades of gray. Higher values for the precipitation index correspond to a confident assessment of surface rainfall. Only the rain / no-rain thresholds (Category 7 in Table 1) vary across the AMPR scan to account for rotating polarization across the AMPR scan. Other thresholds are independent of scan angle.

For rain indices equal to 7 or higher, the index has been generated using one of six TB rain emission tests and one of four TB ice scattering texts. The emission texts are based on increasing 10 GHz TB (i.e., increasing liquid rain). The scattering tests indicate which AMPR wavelength is being scattered by large ice. In general, the larger the ice particles that are present, then the longer the wavelength that will be scattered. This relationship can be used as a surrogate indicator of vigorous convection. If there is

---

[*] *Corresponding Author Address*: Robbie E. Hood, NASA/MSFC Code: SD60, Huntsville, AL, 35812; email: robbie.hood@msfc.nasa.gov.

Table 1. AMPR precipitation index descriptions, criteria, and representative radar reflectivities (median and the range covering the middle 90% of observed values in Hurricanes Bonnie, Erin, and Humberto) .are listed. Many indices are achieved too rarely to estimate representative reflectivities.

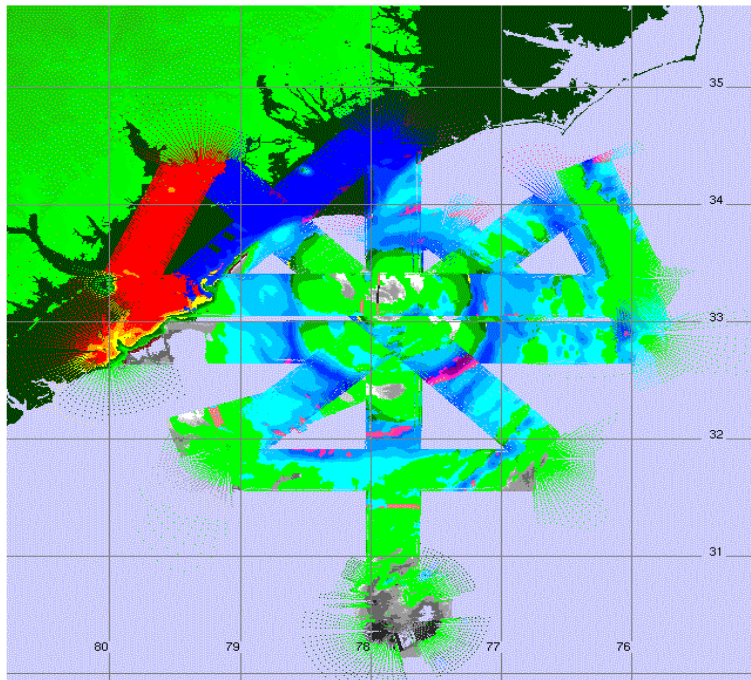| Category	Color	Description	Criteria	3 km dBZ	8 km dBZ
1		Possible cloud	TB85 > 260	<0	<0
2		Possible cloud	TB85 > 265	<0	<0
3		Possible cloud or shallow rain	TB85 > 270	<0	<0
4		Possible cloud or shallow rain	TB85 > 275	<0	<0
7		Shallow, light rain	TB10 > 160 or TB37 > 215	15 (<0-28)	<0
8		Shallow, moderate rain	TB10 > 175	21 (<0-38)	<0
9		Shallow, moderate rain	TB10 > 200	33 (12-41)	9 (<0-17)
10		Shallow, heavy rain	TB10 > 225	na	na
11		Shallow, intense rain	TB10 > 250	na	na
12		Shallow, intense rain	TB10 > 275	na	na
13		Moderate ice, light rain	(7) above; TB85 < TB37; TB85 < 275	29 (15-34)	15 (<0-23)
14		Moderate ice, moderate rain	(8) above; TB85 < TB37; TB85 < 275	32 (20-38)	14 (<0-22)
15		Moderate ice, moderate rain	(9) above; TB85 < TB37; TB85 < 275	35 (27-40)	15 (<0-23)
16		Moderate ice, heavy rain	(10) above; TB85 < TB37; TB85 < 275	38 (30-43)	16 (<0-23)
17		Moderate ice, intense rain	(11) above; TB85 < TB37; TB85 < 275	40 (32-44)	17 (3-25)
18		Moderate ice, intense rain	(12) above; TB85 < TB37; TB85 < 275	na	na
19		Large ice, light rain	(13) above; TB37 < TB19 or TB37 < 1.3*TB85	na	na
20		Large ice, moderate rain	(14) above; TB37 < TB19 or TB37 < 1.3*TB85	na	na
21		Large ice, moderate rain	(15) above; TB37 < TB19 or TB37 < 1.3*TB85	38 (21-43)	19 (14-31)
22		Large ice, heavy rain	(16) above; TB37 < TB19 or TB37 < 1.3*TB85	39 (34-44)	21 (7-29)
23		Large ice, intense rain	(17) above; TB37 < TB19 or TB37 < 1.3*TB85	41 (35-44)	22 (13-34)
24		Large ice, intense rain	(18) above; TB37 < TB19 or TB37 < 1.3*TB85	na	na
25		Intense ice, light rain	(19) above; TB19 < TB10	na	na
26		Intense ice, moderate rain	(20) above; TB19 < TB10	na	na
27		Intense ice, moderate rain	(21) above; TB19 < TB10	na	na
28		Intense ice, heavy rain,	(22) above; TB19 < TB10	na	na
29		Intense ice, intense rain	(23) above; TB19 < TB10	41 (32-43)	32 (22-39)
30		Intense ice, intense rain	(24) above; TB19 < TB10	42 (40-44)	25 (20-31)

Figure 1. Map of AMPR precipitation indices for Hurricane Bonnie, 26 Aug. 1998. See Table 1 for color code.
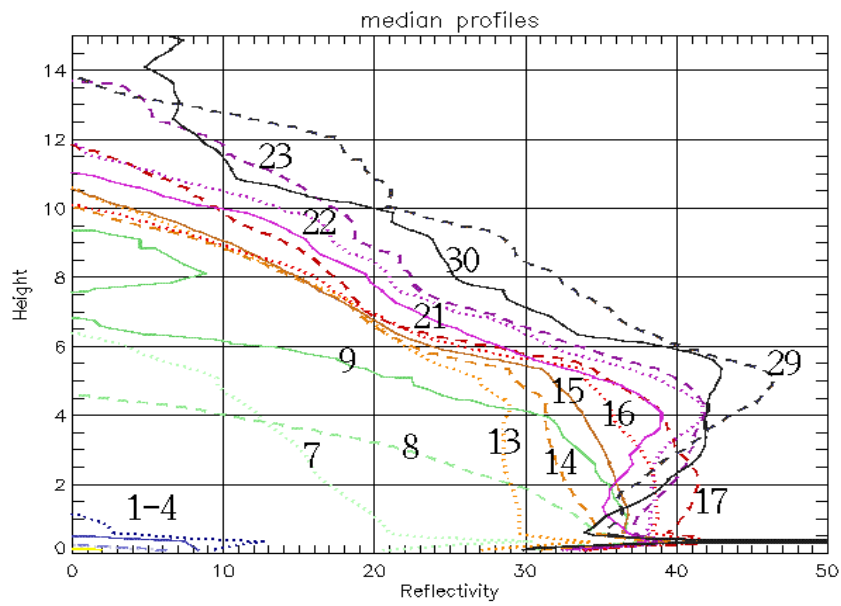

Figure 2. Median profiles of EDOP reflectivity (dBZ) as a function of AMPR precipitation index. Note that colors differ from those in the other figures.

no appreciable scattering (no large ice), the precipitation index has values 7-12 (depending on the emission). These are shades of green in Fig. 1, with darker greens and yellow indicating greater emission (more rain). If only the 85 GHz channel is scattered (ice is large enough to scatter 3.5 mm wavelength radiation), an index of 13-18 is assigned. These are all shades of blue. If ice is large enough to scatter the 37 GHz channel (8.1 mm wavelength), an index of 19-24 is assigned (shades of pink/purple). If ice is large enough to scatter the 19 GHz channel (1.6 cm wavelength), an index of 25-30 is applied. In Fig. 1, this only occurs in a small portion of the outer eyewall in the southeastern quadrant.

In order to better interpret the AMPR precipitation indices, representative vertical profiles of radar reflectivity from the ER-2 Doppler Radar (EDOP) are plotted in Fig. 2. (See in Heymsfield et al. (2001) for a description of EDOP.) These profiles correspond to the median reflectivities at each height. It is evident from Table 1 that there is a great deal of variation about these medians (especially for lower precipitation index values). Nevertheless, these profiles do show a correspondence between emission index and low level reflectivity and between scattering index and upper level reflectivity. For example, profiles 9, 15, and 21 all have the same 10 GHz emission criteria (TB10 > 200 K) and all have reflectivities in the 35-37 dBZ range below 2 km. Profiles 8 and 14 have a lower 10 GHz threshold and consequently lower reflectivities. Profiles 16 and 22 have higher 10 GHz thresholds along with higher reflectivity values below 2 km. At higher altitudes above the freezing level, the profiles cluster together based on their scattering indices.

3. Comparison of Precipitation Types

The following section examines the first ER-2 overpass of the 26 August Hurricane Bonne mission along TRMM satellite data collected at nearly the same time. Fig. 3a displays the AMPR rainfall algorithm using the color scheme defined in Table 1 along with ER-2 data collected as the aircraft flew from the SW at 1158 UTC to NE at 1211 UTC. Fig. 3b is a simplification of the AMPR rainfall algorithm to highlight convective rain in red, stratiform rain in green, and ambiguous rain types of either stratiform or shallow convection in gold.

Figs 4 and 5 displays TRMM satellite products representing Hurricane Bonnie rainfall patterns at 1134 UTC. The black rectangular outline in each of these figures highlights the position of the corresponding AMPR information displayed in Fig. 3a and 3b. Fig. 4a maps the TRMM 2A12 surface rain rate in mm/hr derived using TMI information. Fig. 4b represents the percentage of convective surface rain derived from a TRMM 2A12 convective rain rate product not shown here. Fig. 5a shows the TRMM 2A25 PR reflectivity at 3 km altitude while Fig. 5b maps the same reflectivity product at 8 km altitude.

Fig. 6 displays the TRMM 2A23 rain type classification derived using PR observations to highlight convective rain in red and stratiform in green.

There was substantial evolution of the Hurricane Bonnie during the mission, which accounts for qualitative differences between the structure seen in AMPR information shown in Fig. 1 and TRMM products displayed in Figs. 4 and 5. Notably, the strong convection initially on the northern side of the storm rotated around to the southeastern side as observed in WSR-88D data collected by the Wilmington radar

The classification of rain in Fig 3a indicates most of the swath is dominated by shallow light rain that matches with the PR reflectivity patterns at 3 and 8 km in Fig 5. The deeper ice regions on the SW end of the AMPR swath also correlate with the PR reflectivities at 8 km.

The AMPR convective-stratiform product displayed in Fig. 3b shows an area of convection in the SW end of the swath. This corresponds to a similar convection in Fig 4b although the area is much more widespread. While the AMPR product also indicates stratiform rain in this area, the TRMM 2A12 in Fig. 4b displays widespread convective rain contributing to over 60% of the rain total. This discrepancy requires further study, but one reason may be due to an over-reliance on ice scattering signatures in the TRMM algorithm.

The TRMM (PR) convective-stratiform product in Fig 6 agrees fairly well with the AMPR product in the SW area and rain-free areas. Although the NE sector of the PR product indicates convection where AMPR product does not, the PR reflectivities in Fig 5 at 3 and 8 km do not appear highly convective. These differences may be in part due to the time lag (~20 mins) between the AMPR and TRMM observations.

4. Summary

The four frequencies of passive microwave information collected by the AMPR during CAMEX-3 can be used to provide qualitative descriptions of the hydrometeor structure of hurricane precipitation features. A preliminary comparison of these airborne rain products has been conducted with space-based rain products derived from TRMM observations for a small sample of 1998 Hurricane Bonnie data. Many more tropical cyclone and other tropical rain systems will be examined as the investigation progresses. Analysis of other auxiliary information such as radar and lightning must also be completed before quantitative interpretations of the AMPR information may be performed. Yet, this type of analysis offers a path to identifying uncertainties in space-based tropical cyclone rainfall estimation and convective intensity characterizations.
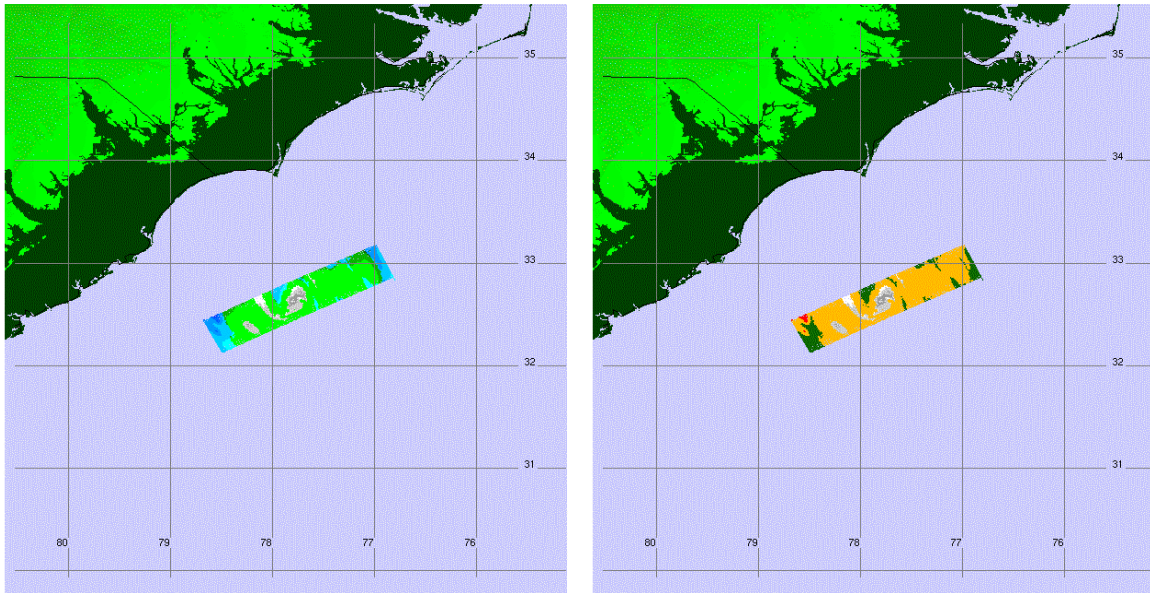
Fig. 3: AMPR pass over Bonnie on 26 Aug 1998 at 1158 UTC (SW) to 1211UTC (NE). a. Rainfall algorithm results (refer to Table 1 for identifiers), and b. Rainfall algorithm interpreted as convective (red), stratiform (green), and either shallow convective or stratiform (gold).

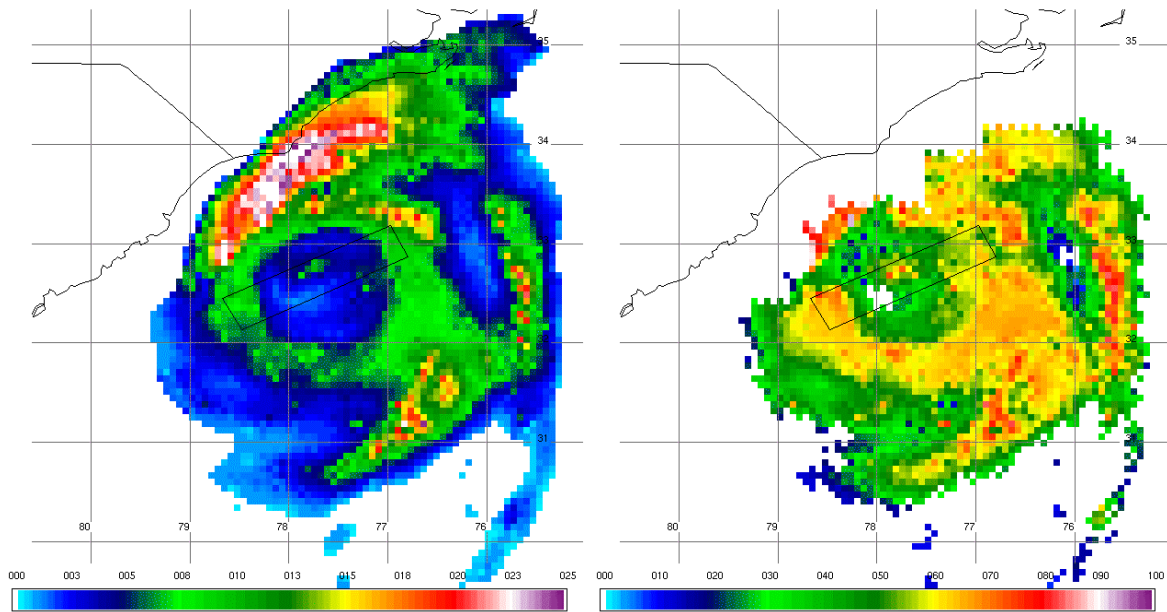2A12 SURFACE RAIN   2A12 PERCENT CONVECTIVE SURFACE RAIN

Fig 4: TRMM satellite overpass of hurricane Bonnie at 1135 UTC for TMI 2A12 products, a. surface rain in mm/hr, and b. derived percent convective surface rain.

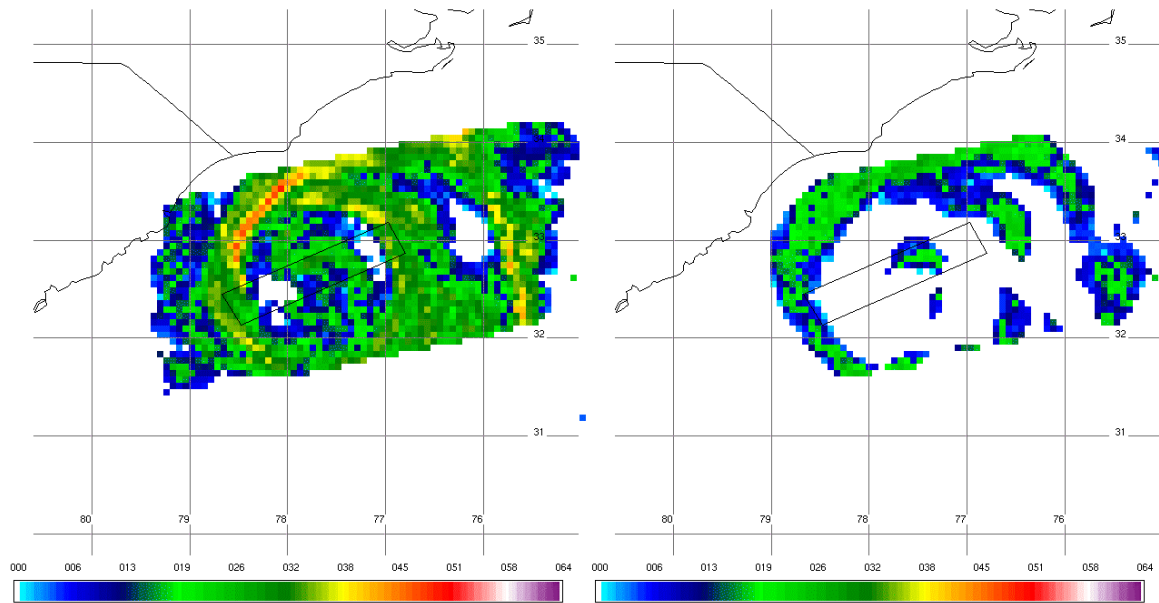2A25 CORR Z 3KM   2A25 CORR Z 8KM

Fig 5: TRMM satellite overpass of hurricane Bonnie at 1135 UTC for PR 2A25 product reflectivity (Z) at a. 3 km, and
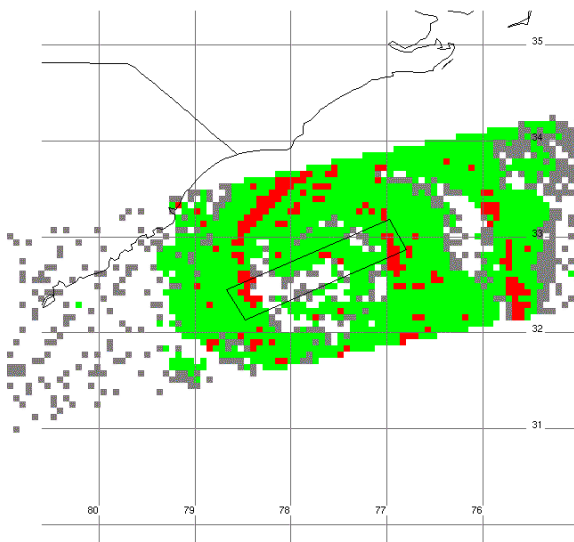b. 8 km.

2A23 RAIN TYPE

Fig 6: TRMM satellite overpass of hurricane Bonnie at 1135 UTC for PR 2A23 product rain type. Convective rain in
red and stratiform rain in green.

5. Acknowledgements

6. References

Asrar, G., J.A. Kaye, and P. Morel, 2001: NASA research strategy of Earth system Science: Climate Component. *Bull. Amer. Meteor. Soc.*, 82, 1309-1329.

Elsberry, R.L., 2002: Predicting Hurricane Landfall Precipitation: Optimistic and Pessimistic Views from the Symposium on Precipitation Extremes. *Bull. Amer. Meteor. Soc.,* **83**, 1333-1339.

Kummerow, C. and Coauthors, 2000: The status of the Tropical Rainfall Measuring Mission (TRMM) after two years in orbit. *J. Appl. Meteor.,* **39**, 1965-1982.

Heymsfield, G.M., J.B. Halverson, J. Simpson, L. Tian, and T.P. Bui, 2001: ER-2 Doppler radar investigations of the eyewall of Hurricane Bonnie during the Convection and Moisture Experiment-3. *J. Appl. Meteor.,* **40**, 1310-1330.

Spencer, R.W., R.E. Hood, F.J. LaFontaine, E.A. Smith, R. Platt, J. Galliano, V.L.Griffin, and E. Lobl, 1994: High resolution imaging of rain systems with the Advanced Microwave Precipitation Radiometer. *J. Atmos. Oceanic Technol.,* **11**, 849-857.